Is shrub expansion into grasslands pushed or pulled? A spatial integral projection model for woody plant encroachment

Trevor Drees*[a,b], Brad M. Ochocki[b], Scott L. Collins[c], and Tom E.X. Miller[b]

[a]Department of Biology, Penn State University, State College, PA USA

[b]Program in Ecology and Evolutionary Biology, Department of BioSciences, Rice University, Houston, TX USA

[c]Department of Biology, University of New Mexico, Albuquerque, NM USA

April 20, 2022

*thd5066@psu.edu

Abstract

Encroachment[1] of shrubs into adjacent grasslands has become an increasingly reported phenomenon across the world, and such encroachment is either pulled forward by high population growth at the low-density encroachment front or pushed forward by higher-density areas behind the front. However, at sites such as Sevilleta National Wildlife Refuge in central New Mexico, little is known about whether encroachment is pushed or pulled, and the dynamics of encroachment are not well-understood. Here, long-term encroachment of creosotebush (Larrea tridentata), a native perennial shrub, stands in stark contrast with the stagnation in encroachment observed in recent decades. In order to better understand creosotebush encroachment at this site, we quantify it using a spatially structured population model where a wave of individuals travels at a speed governed by both dispersal and density-dependence. Results indicate that population growth rates generally increase with decreasing density, suggesting that encroachment is pulled by individuals at the low-density wave front, and the spatial population model predicts an encroachment rate of less than 2 cm per year. While the predicted rate of encroachment is consistent with observations over recent decades, it does not explain long-term creosotebush encroachment at the study site, suggesting that this process may occur in pulses when recruitment, seedling survival, or dispersal significantly exceed typical rates. Overall, our work demonstrates that individuals at low densities are likely the biggest contributors to creosotebush encroachment at this site, and that this encroachment is likely a process that occurs in large but infrequent bursts rather than at a steady pace.

Keywords

density-dependence, ecotones, woody encroachment, shrubs, integral projection model, grassland

---

[1] *I am not editing the abstract for now.*

Introduction

The recent and ongoing encroachment of shrubs and other woody plants into adjacent grasslands has caused significant vegetation changes across arid and semi-arid landscapes worldwide (Van Auken, 2000, 2009; Goslee et al., 2003; Gibbens et al., 2005; Parizek et al., 2002; Cabral et al., 2003; Trollope et al., 1989; Roques et al., 2001). The process of encroachment generally involves increases in the number or density of woody plants in both time and space (Van Auken, 2000), which can drive shifts in plant community structure and alter ecosystem processes (Schlesinger et al., 1990; Ravi et al., 2009; Schlesinger and Pilmanis, 1998; Knapp et al., 2008). Other effects of encroachment include changes in ecosystem services (Reed et al., 2015; Kelleway et al., 2017), declines in biodiversity (Ratajczak et al., 2012; Sirami and Monadjem, 2012; Brandt et al., 2013), and economic losses in areas where the proliferation of shrubs adversely affects grazing land and pastoral production (Mugasi et al., 2000; Oba et al., 2000).

Woody plant encroachment can be studied through the lens of spatial population biology as a wave of individuals that may expand across space and over time (Kot et al., 1996; Neubert and Caswell, 2000; Wang et al., 2002; Pan and Lin, 2012). Theory predicts that the speed of wave expansion depends on two processes: local demography and dispersal of propagules. First, local demographic processes include recruitment, survival, growth, and reproduction, which collectively determine the rate at which newly colonized locations increase in density and produce new propagules. Second, colonization events are driven by the spatial dispersal of propagules, which is commonly summarized as a probability distribution of dispersal distance, or "dispersal kernel". The speed at which expansion waves move is highly dependent upon the shape of the dispersal kernel, especially long-distance dispersal events in the tail of the distribution (Skarpaas and Shea, 2007). Both demography and dispersal may depend on plant size, since larger plants often have improved demographic performance and release seeds from greater heights,

3

leading to longer dispersal distances (Nathan et al., 2011). Accounting for population structure, including size structure, may therefore be important for understanding and predicting wave expansion dynamics (Neubert and Caswell, 2000).

Theory predicts that the nature of conspecific density dependence is another critical feature of expansion dynamics but this is rarely studied in the context of woody plant encroachment. Expansion waves typically correspond to gradients of conspecific density – high in the back and low at the front – and demographic rates may be sensitive to density due to intraspecific interactions like competition or facilitation. If the demographic effects of density are strictly negative due to competitive effects that increase with density then demographic performance is maximized as density goes to zero, at the leading edge of the wave. Under these conditions, the wave is "pulled" forward by individuals at the low-density vanguard (Kot et al., 1996), and targeting these individuals and locations would be the most effective way to slow down or prevent encroachment (cite?). However, woody encroachment systems often involve positive feedbacks whereby shrub establishment modifies the environment in ways that facilitate further shrub recruitment. For example, woody plants can modify their micro-climates in ways that elevate nighttime minimum temperatures, promoting conspecific recruitment and survival for freeze-sensitive species (D'Odorico et al., 2010; Huang et al., 2020). Positive density dependence (or Allee effects) causes demographic rates to be maximized at higher densities behind the leading edge, which "push" the expansion forward, leading to qualitatively different expansion dynamics (Kot et al., 1996; Taylor and Hastings, 2005; Sullivan et al., 2017; Lewis and Kareiva, 1993; Veit and Lewis, 1996; Keitt et al., 2001). Pushed expansion waves generally have different shapes (steeper density gradients) and slower speeds than pulled waves (Gandhi et al., 2016), and may require different strategies for managing or decelerating expansion (check Taylor and Hastings ref). The potential for positive feedbacks is well documented in woody encroachment systems but it remains unclear whether and how strongly these feedbacks decelerate shrub expansion and influence

4

strategies for management of woody encroachment.

In this study, we linked woody plant encroachment to ecological theory for invasion waves, with the goals of understanding how seed dispersal and density-dependent demography drive encroachment, and determining whether the encroachment wave is pushed or pulled. Throughout the aridlands of the southwestern United States, shrub encroachment into grasslands is well documented (cite) but little is known about the dispersal and demographic processes that govern it. Our work focused on encroachment of creosotebush (*Larrea tridentata*) in the northern Chihuahuan Desert. Expansion of this species into grasslands over the past 150 years has been well documented, leading to decreased cover of *Bouteloua eriopoda*, the dominant foundation species of Chihuahuan desert grassland (Gardner, 1951; Buffington and Herbel, 1965; Gibbens et al., 2005). As in many woody encroachment systems, creosotebush expansion generates ecotones marking a transition from dense shrubland to open grassland, with a transition zone in between where shrubs can often be found interspersed among grasses (Fig. 1).
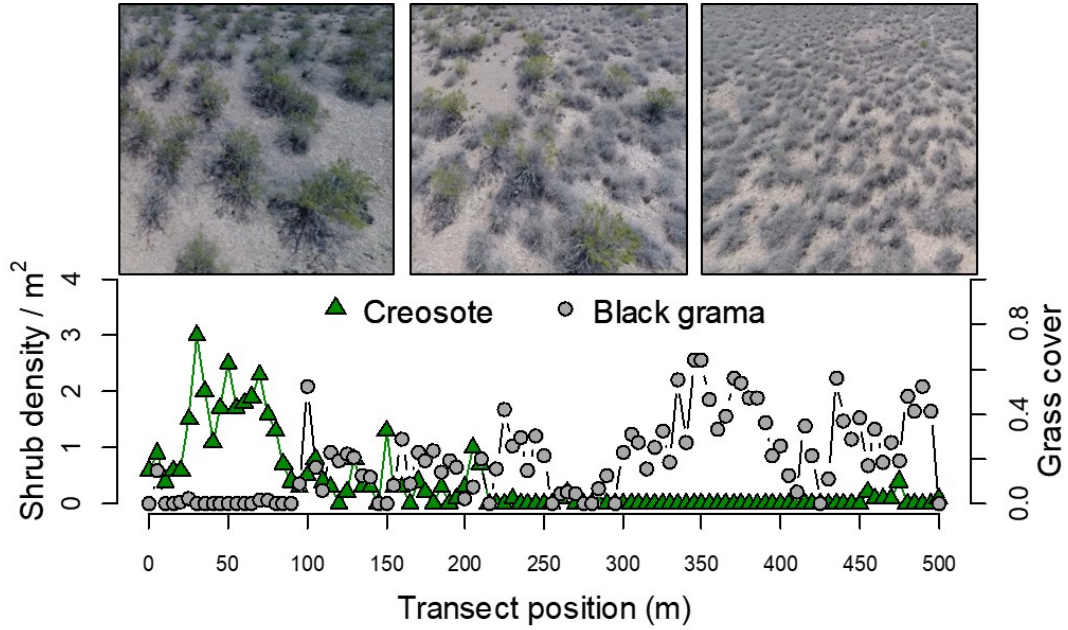
Figure 1: Example of an ecotone transect at Sevilleta LTER, spanning gradients of creosotebush and black grama grass.

Historically, creosotebush encroachment into grasslands is believed to have been driven by a combination of factors including overgrazing, drought, variability in rainfall, and suppression of fire regimes Moreno-de las Heras et al. (2016). These shrubs are also thought to further facilitate their own encroachment through positive feedbacks (Grover and Musick, 1990; D'Odorico et al., 2012) by modifying their environment in ways that favor continued growth and recruitment, including changes to the local micro-climate (D'Odorico et al., 2010) and rates of soil erosion (Turnbull et al., 2010). Such positive feedback also involve suppression of herbaceous competitors, reducing competition as well as the amount of flammable biomass used to fuel the fires that keep creosotebush growth in check (Van Auken, 2000). We hypothesized that, given potential for positive feedback mechanisms, the rarity of conspecifics at the low-density encroachment front may depress demographic performance and generate pushed-wave dynamics.

6

We used a combination of observational and experimental data from shrub ecotones in central New Mexico to parameterize a spatial integral projection model (SIPM) that predicts that speed of encroachment (m/yr) resulting from lower-level demographic and dispersal processes. Our data came from demographic surveys and experimental transplants along replicate ecotone transects spanning a gradient of shrub density, and seed drop experiments to infer the properties of the dispersal kernel. We focused on wind dispersal of seeds as a starting point, since little is known about the natural history of dispersal in this system and the seeds lack rewards to attract animal dispersers. We also used re-surveys of permanents transects as an independent measure of encroachment that provided a benchmark against which to evaluate model predictions. The SIPM accounts for size-structured demography of creosotebush, allows us to test whether shrub expansion is pulled by the low-density front or pushed from the high-density core, and identifies the local (demographic) and spatial (seed dispersal) life cycle transitions that most strongly contribute to expansion speed[2]. We address the following specific questions:

1. What is the observed rate of creosotebush encroachment in recent past?

2. How do creosotebush size and conspecific density affect variation in demographic vital rates (survival, growth, reproduction, and recruitment) along shrub encroachment ecotones?

3. What is the wind dispersal kernel for this species and how far do seeds typically travel by wind?

4. What is the predicted rate of expansion from the SIPM and what lower-level processes most strongly govern the expansion speed?

---

[2]*we will need to stay consistent with the language of encroachment/expansion/invasion. For now I am swictihg a lot.*

5. Is encroachment pulled by the individuals at the front of the wave or pushed by individuals behind it?

Materials and methods

Study species

Creosotebush *Larrea tridentata* is a perennial, drought-resistant shrub that is native to the arid and semiarid regions of the southwestern United States and northern Mexico. High-density areas of creosotebush consist largely of barren soil between plants due to the "islands of fertility" these shrubs create around themselves (Schlesinger et al., 1996; Reynolds et al., 1999), though lower-density areas will often contain grasses in the inter-shrub spaces (Fig. 1). In our northern Chihuahuan desert study region creosotebush reproduces sexually, with numerous small yellow flowers giving rise to highly pubescent spherical fruits several millimetres in diameter; these fruits consist of five carpels, each of which contains a single seed. Seeds are dispersed from the parent plant by gravity and wind, with the possibility for seeds to also be blown across the soil surface or trans-ported by water runoff (Maddox and Carlquist, 1985). In other regions, this species also reproduces asexually and can give rise to long-lived clonal stands (Vasek, 1980), but this does not occur in our study region. The foliage is dark green, resinous, and unpalatable to most grazing and browsing animals (Mabry et al., 1978).

Study site

We conducted our experiments and censuses at the Sevilleta National Wildlife Refuge (SNWR), a Long-Term Ecological Research (LTER) site in central New Mexico. The refuge exists at the intersection of several eco-regions, including the Chihuahuan Desert and steppes of the Colorado Plateau. Annual precipitation is low at approximately 250 mm, with the majority falling during the summer monsoon season from June to

8

September.

Significant creosotebush encroachment at SNWR last occurred in the 1950's, with high shrub recruitment before and after a multi-year drought that caused a large loss in grass cover, likely setting the stage for creosotebush expansion (Moreno-de Las Heras et al., 2015; Moreno-de las Heras et al., 2016). The recruitment events that facilitate creosotebush expansion are thought to be highly episodic (Peters and Yao, 2012). Given that creosotebush seedlings have been shown to establish around the time that late-summer heavy rainfall occurs (Boyd and Brum, 1983; Bowers et al., 2004), higher precipitation rates may be responsible for increased recruitment.

Encroachment re-surveys

We recorded shrub percent cover along two permanent 1000-m transects that spanned the shrub-grass ecotone, from high to low to near-zero shrub density. These surveys were conduced in summer 2001 and again in summer 2013 to document change in creosotebush abundance and spatial extent. At every 10 meters, shrub cover was recorded in nine cover classes (<1%, 1–4%, 5–10%, 10–25%, 25–33%, 33–50%, 50–75%, 75–95%, >95%). For visualization, we show midpoint values of these cover classes at each meter location for both transects and years.

Demographic data

Ecotone transects

Collection of demographic data occurred during early June of every year from 2013-2017. This work was conducted at four sites in the eastern part of SNWR (one site was initiated in 2013 and the other three in 2014), with three transects at each site (different transects than those used for re-surveys). All transects were placed along a shrubland-grassland ecotone so that a full range of shrub densities was captured: each transect spanned core shrub areas, grassland with few shrubs, and the transition between them. Lengths

of these transects varied from 200 to 600 m, determined by the strength of vegetation transition since "steep" transitions required less length to capture the full range of shrub densities.

We quantified shrub density in 5-meter "windows" along each transect, including all shrubs within one meter of the transect on either side. Densities were quantified once for each transect (in 2013 or 2014) and were assumed to remain constant for the duration of the study, a reasonable assumption for a species with very low recruitment and very high survival of established plants. Given the population's size structure, we weighted the density of each window by the sizes of the plants, which we quantified as volume (cm^3). Volume was calculated as that of an elliptic cone: $V_i = \frac{\pi h}{3} \frac{lw}{4}$ where l, w, and h are the maximum length, maximum width, and height, respectively. Maximum length and width were measured so that they were always perpendicular to each other, and height was measured from the base of the woody stem at the soil surface to the highest part of the shrub. The weighted density for a window was then expressed as log(volume) summed over all plants in the window.

Observational census

At 50-m intervals along each transect we tagged up to 10 plants for annual demographic census and recorded their local (5-m resolution) window so that we could connect individual demographic performance to local weighted density. These tagged shrubs were revisited every June and censused for survival (alive/dead), size (width, length, and height, as above), and reproduction (numbers of flowers and fruits). In instances where shrubs had large numbers of reproductive structures that would be difficult to reliably count (a large shrub may have thousands of flowers or fruits), we made counts on a fraction of the shrub and extrapolated to estimate whole-plant reproduction. Creosotebush does not have a discrete reproductive season, instead producing flowers and fruits over much of the warm season. Our measurements of reproductive output are therefore con-

10

servative, and likely underestimate cumulative seed production for an entire transition year. Each year, we searched for new recruits within one m on either side of the transect. New recruits were tagged and added to the demographic census.

Transplant experiment

We conducted a transplant experiment in 2015 to test how shrub density affects seedling survival. This approach complemented observational estimates of density dependence and filled in gaps for a part of the shrub life cycle that is rarely observed due to low recruitment. Seeds for the experiment were collected from plants in our study population in 2014. Seeds were germinated on Pro-Mix potting soil (Quakertown, PA) in Fall 2014 and seedlings were transferred to 3.8 cm-by-12.7 cm cylindrical containers and maintained in a greenhouse at Rice University. Seedlings were transported to SNWR and transplanted into our experimental design during July 27-31, 2015. Transplant timing was intended to coincide with the start of the monsoon season, when most natural recruitment occurs.

The transplant experiment was conducted at the same four sites and three transects per site as the observational demographic census, where we knew weight shrub densities at 5-m window resolution. Along each transect we established 12 1-m by 1-m plots. Plots were intentionally placed to capture density variation: four plots were in windows with zero shrubs, four plots were placed in the top four highest-density windows on the transect, and the remaining four plots were randomly distributed among the remaining windows with weighted density greater than zero. Plots were placed in the middle of each 5-m window (at meter 2.5) and were divided into four 0.5-m by 0.5-m subplots. We divided each subplot into nine squares and recorded ground cover of each square as one of the following categories: bare, creosotebush, black grama (*B. eriopoda*), blue grama (*B. gracilis*), other grass, or "other". Each subplot received one transplanted subplot, for a total of 48 transplants per transect, 144 transplants per site, and 576 transplants in the entire experiment. Each site was set up on a different day and there was a significant

monsoon event after the third and before the fourth site. This resulted in differential mortality that appears to be related to site (the soil was moist at the fourth site at the time of transplanting, which favored survival) but more likely reflects the timing of the monsoon event relative to planting. We revisited the transplant experiment on October 24, 2015 to survey mortality. After that first visit, transplants were censused along with the naturally occurring plants each June, following the methods described above.

Demographic analysis

We fit statistical models to the demographic data and used AIC-based model selection to evaluate empirical support for alternative candidate models. The top statistical models were then used as the vital rate sub-models of the SIPM, so there is a strong connection between the statistical and population modeling, as is typical of integral projection modeling. Our analyses focused on the following demographic vital rates: survival, growth, probability of flowering, flower and fruit production, and seedling recruitment. All of these except recruitment were modeled as a function of plant size, and all of them included the possibility of density dependence, since we could connect the demographic performance of individual shrubs to the weighted density of their transect window.

The alternative hypotheses of pushed versus pulled wave expansion rest on how demographic vital rates, and the rate of population increase (λ) derived from the combination of all vital rates, respond to density. We were particularly interested in whether demographic performance was maximized as local density goes to zero (pulled) or at non-zero densities behind the wave front (pushed). To flexibly model density dependence and detect non-monotonic responses, we used generalized additive models in the R package 'mgcv' (Wood, 2017). For each vital rate, we fit candidate models with or without a smooth term for local weighted density (among other possible covariates). To avoid over-fitting, we set the 'gamma' argument of gam() to 1.5, which increases the complexity penalty, results in smoother fits (Wood, 2017), and makes our approach more

12

conservative (other gamma values yielded qualitatively similar results). We pooled data across transition years for analysis. All models included the random effect of transect (12 transects across 4 sites); we did not attempt to model both site and transect-within-site random effects due to the low numbers of each. All vital rate functions used the natural logarithm of volume (cm^3) as the size variable and the sum log(volume) as the weighted density of a transect window.

Survival   We modeled survival or mortality in year $t+1$ as a Bernoulli random variable with three candidate models for survival probability. These included smooth terms for initial size in year t only (1), initial size and weighted density (3), and both smooth terms plus an interaction between initial size and weighted density. We analyzed survival of experimental transplants and observational census plants together in the same analyses, with a fixed effect of 'transplant' included in all candidate models. Since recruits and thus mortality events were both very rare in the observational survey, this approach allowed us to "borrow strength" over both data sets to generate a predictive function for size- and possibly density-dependent survival while statistically accounting for differences between experimental and naturally occurring plants. Because we had additional, finer-grained cover data for the transplant experiment that we did not have for the observational census, we conducted an additional stand-alone analysis of transplant survival that explored the influence of covariates at multiple spatial scales (Appendix).

Growth   We initially modeled size in year $t+1$ as a Gaussian random variable. There were nine candidate models for growth (Table). The simplest model (1) defined the mean of size in year $t+1$ as a smooth function of size in year t and constant variance. Models (2) and (3) had constant variance but the mean included smooth terms for initial size and weighted density (2) or both smooth terms plus an interaction between initial size and weighted density (3). Models 4-6 had the same mean structure as 1-3 but defined the standard deviation of size in year $t+1$ as a smooth function of initial size. Models

13

7-9 mirrored 4-6 and additionally included a smooth term for weighted density in the standard deviation.

Inspection of the best-fitting growth model suggested that the data did not conform well to a Gaussian distribution: there was excess kurtosis (fatter tails) relative to Gaussian and left skew in the distribution of size in year $t+1$ especially at small initial sizes. Therefore, we re-fit the growth model with a skewed generalized t (sgt) distribution, a five-parameter distribution on the real line that accommodates excess kurtosis and skew (R package 'sgt': (Davis, 2015)). We specified μ and σ of the sgt using the basis functions generated by the best-fit gam, and additionally modeled the λ parameter (which controls skewness) as a function of size in year t and the p and q parameters (which control kurtosis) as constants. We verified that the sgt model described the data well by simuating data from it and comparing simulated and real data (Appendix Fig).

Flowering and fruit production   We modeled shrub reproductive status (vegetative or flowering) in year t as a Bernoulli random variable with three candidate models for flowering probability. These included smooth terms for current size (in year t) only (1), size and weighted density (3), and both smooth terms plus an interaction between size and weighted density. We modeled the reproductive output of flowering plants (the sum of flowerbuds, open flowers, and fruits – assuming that all of these equally contribute to overall seed production) in year t as a negative binomial random variable. There were three candidate models for mean reproductive output that corresponded to the same three candidates for flowering probability.

Recruitment   We modeled seedling recruitment in each transect window as a binomial random variable given the number of total seeds produced in that window in the preceding year. To estimate window-level seed production, we used the best-fit models for flowering and fruit production and applied this to all plants in each window that we observed in our initial density surveys.

14

Density-dependent IPM

The size- and density-dependent statistical models comprised the sub-models of a density dependent Integral Projection Model that we used to evaluate how the shrub population growth rate responded to conspecific density; we present this non-spatial model before layering on the spatial dynamics driven by seed dispersal. A basic density-independent IPM predicts the number of individuals of size $x\prime$ at time $t+1$ ($n(x\prime, t+1)$) based on a projection kernel (K) that gives the rates of transition from sizes x to $x\prime$ from times t to $t+1$ and is integrated over the size distribution from the minimum (L) to maximum (U) sizes. In a density-dependent IPM, components of the projection kernel may respond to population abundance and structure:

$$n(x\prime, t+1) = \int_L^U K(x\prime, x, \tilde{n}(t)) n(x, t)\, dx \tag{1}$$

Here, $\tilde{n}(t)$ is some function of population structure $n(x, t)$ such as the total density of conspecifics ($\tilde{n}(t) = \int n(x, t)\, dx$) or, as in our case, total density weighted by size ($\tilde{n}(t) = \int x n(x, t)\, dx$). For simplicity, in the analyses that follow we do not model density as a dynamic state variable; instead, we treat density as a static covariate ($\tilde{n}(t) = \tilde{n}$) and evaluate the IPM at a range of density values. As in our statistical modeling, the size variable of the IPM ($x, x\prime$) was $log(cm^3)$.

For our model, the size- and density-dependent demographic transitions captured by the projection kernel include growth or shrinkage (g) from size x to $x\prime$ conditioned on survival (s) at size x (combined growth-survival function $G(x\prime, x, \tilde{n}) = g(x\prime, x, \tilde{n}) s(x, \tilde{n})$), and the production of new size-$x\prime$ individuals from size-x parents ($Q(x\prime, x, \tilde{n})$). Reproduction reflects the probability of flowering at size x (p), the number of seeds produced by flowering plants (d), the per-seed probability of recruitment (r), and the size distribution of recruits (c). Collectively, the rate at which x-sized individuals produce $x\prime$-sized individuals at density $\tilde{n}$ is given by the combined reproduction-recruitment function

15

331    $Q(x\prime, x, \tilde{n}) = p(x, \tilde{n})d(x, \tilde{n})r(\tilde{n})c(x\prime)$. Thus, we can express the projection kernel as:

$$K(x\prime, x, \tilde{n}) = G(x\prime, x, \tilde{n}) + Q(x\prime, x, \tilde{n}) \tag{2}$$

333   In the statistical modeling we explored local density effects in all of these vital rates

334 except the recruit size distribution $c(x\prime)$. We observed only 32 natural recruits, so we

335 were not able to connect recruit size to local density. Instead, we used the pooled re-

336 cruits to estimate a mean and standard deviation of recruit size assuming a Gaussian

337 distribution. For analysis, we evaluated the IPM kernel over a range of local densities

338 from the minimum to the maximum of weighted density values from the 5-meter win-

339 dows ($0 \leq \tilde{n} \leq \tilde{n}_{max}$). At each density level, we discretized the IPM kernel into a

340 200×200 approximating matrix and calculated the asymptotic growth rate $\lambda(\tilde{n})$ as its

341 leading eignevalue. We extended the lower (L) and upper (U) integration limits to avoid

342 unintentional "eviction" using the floor-and-ceiling method (Williams et al., 2012).

343   We sought to characterize the shape of density dependence: whether fitness declined

344 monotonically or not with increasing density. We quantified uncertainty in the density-

345 dependent growth rate $\lambda(\tilde{n})$ by bootstrapping our data. For each bootstrap, we randomly

346 sampled 75% of our demographic data, re-ran the statistical modeling and model selec-

347 tion, and used the top vital rate models to generate $\lambda(\tilde{n})$ for that data subset. We

348 repeated this procedure for 500 bootstrap replicates.

Dispersal modelling

350 **WALD dispersal model**   Dispersal kernels were calculated using the WALD, or Wald

351 analytical long-distance dispersal, model that uses a mechanistic approach to predict dis-

352 persal patterns of plant propagules by wind. The WALD model, which is largely based

353 in fluid dynamics, can serve as a good approximation of empirically-determined dispersal

354 kernels (Katul et al., 2005; Skarpaas and Shea, 2007) and may be used when empirical

dispersal data is not readily available. Under the assumptions that wind turbulence is low, wind flow is vertically homogenous, and terminal velocity is achieved immediately upon seed release, the WALD model simplifies a Lagrangian stochastic model to create a dispersal kernel that estimates the likelihood a propagule will travel a given distance (Katul et al., 2005). This dispersal kernel takes the form of the inverse Gaussian distribution

$$p(r) = \left(\frac{\lambda'}{2\pi r^3} \right)^{\frac{1}{2}} \exp \left[-\frac{\lambda'(r - \mu')^2}{2\mu'^2 r} \right] \tag{3}$$

that is a slight adaptation from equation 5b in Katul et al. (2005), using r to denote dispersal distance. Here, λ' is the location parameter and μ' is the scale parameter, which depend on environmental and plant-specific properties of the study system. The location and scale parameters are defined as $\lambda' = (H/\sigma)^2$ and $\mu' = HU/F$; these are functions of the height H of seed release, wind speed U at seed release height, seed terminal velocity F, and the turbulent flow parameter σ that depends on both wind speed and local vegetation roughness.

In order to create the dispersal kernel, we first take the wind speeds at measurement height z_m and correct them to find wind speed U for any height H by using the logarithmic wind profile

$$U = \frac{1}{H} \int_{d+z_0}^{H} \frac{u^*}{K} \log \left(\frac{z - d}{z_0} \right) dz \tag{4}$$

given in Bullock et al. (2012) equation 6, with the notation slightly modified. Here, z is the height above the ground, K is the von Karman constant, and u^* is the friction velocity. The zero-plane displacement d and roughness length z_0 are surface roughness parameters that, for a grass canopy height h above the ground, are approximated by $d \approx 0.7h$ and $z_0 \approx 0.1h$. These estimates are from Raupach (1994) for a canopy area index $\Lambda = 1$ in which the sum of grass canopy elements is equal to the unit area being measured. A 0.15 m grass height at the study site gives $d = 0.105$ and z_0, which are

17

suitable approximations for grassland (Wiernga, 1993). Calculations of u^* were done using equation A2 from Skarpaas and Shea (2007), in which

$$u^* = KU_m \left[\log \left(\frac{z_m - d}{z_0} \right) \right]^{-1} \tag{5}$$

and U_m is the mean wind velocity at the measurement height z_m. Values for the turbulent flow parameter σ were then calculated using the estimate made by Skarpaas and Shea (2007) in their equation A4, where

$$\sigma = 2A_w^2 \sqrt{\frac{K(z-d)u^*}{C_0 U}} \tag{6}$$

and C_0 is the Kolmogorov constant. A_w is a constant that relates vertical turbulence to friction velocity and is approximately equal to 1.3 under the assumptions of above-canopy flow made by Skarpaas and Shea (2007), based off calculations from Hsieh and Katul (1997). In addition, the assumption that $z = H$ was made in order to make the calculation of σ more feasible.[3]

The values from the previous three equations give us the necessary information to calculate μ' and λ', thus allowing us to create the WALD distribution $p(r)$. However, the base WALD model does not take into account variation in wind speeds or seed terminal velocities, which limits its applicability in systems where such variation is present. In order to account for this variation, we integrate the WALD model over distributions these two variables using the same method as Skarpaas and Shea (2007). The WALD model assumes seed release from a single point source, though, which is not realistic for a shrub; because seeds are released across the entire height of the shrub rather than from a point source, $p(r)$ was also integrated across the uniform distribution from the grass canopy height to the shrub height. Thus, under the assumptions that the height at which a seed is located does not affect its probability of being released and that seeds are evenly

---

[3] *Can you describe this assumption in biological terms?*

distributed throughout the shrub, this gives the dispersal kernel $K(r)$, where

$$K(r) = \iiint p(F)p(U)p(z)p(r) \, dF \, dU \, dz \tag{7}$$

and $p(F)$ and $p(U)$ are the PDFs of the terminal velocity F and wind speed U, respectively, and $p(z)$ is the uniform distribution from h to H.

Dispersal data collection The distribution $p(F)$ in the integral above was constructed using experimentally determined seed terminal velocities. This was done by using laboratory-based seed release experiments with a high-speed camera and motion tracking software to determine position as a function of time. We then used the Levenberg-Marquardt algorithm to solve a quadratic-drag equation of motion for F. Before seeds were released, they were dried, dyed with yellow fluorescent powder, and then put against a black background to improve visibility and make tracking easier. While the powder added mass to the seeds, this added mass only yielded an approximately 2.5% increase, likely having little effect on terminal velocities. Measurements were conducted for 48 seeds that were randomly chosen from a seed pool derived from different plants, and then an empirical PDF of terminal velocities was constructed using the data. Constructing $p(U)$ involved creating an empirical PDF of hourly wind speeds using data from a Sevilleta LTER meterological station (Five Points), the station closest to our transects. We used wind speed data collected from 1988 to 2010.[4]

Spatial integral projection model

We used a spatial integral projection model to piece together seed dispersal and density-dependent demography, and generate predictions for the rate of shrub expansion that results from this combination of local and spatial processes. The spatially explicit model builds upon the non-spatial model (Eq. 1) and adds a spatial variable (z, z') such

---

[4] *Most SEV data sets have a doi, so ideally we should cite the wind speed data.*

19

that demographic transitions occur across both time and space according to a combined

demography-dispersal kernel $\tilde{K}$:

$$n(x\prime, z\prime, t+1) = \int_{-\infty}^{+\infty} \int_{L}^{U} \tilde{K}(x\prime, x, z\prime, z, \tilde{n}(z,t)) n(x,z,t) \, dx \, dz \tag{8}$$

Here, $\tilde{K}(x\prime, x, z\prime, z, \tilde{n}(z,t))$ is the rate of transition from size x and location z to size $x\prime$

and location $z\prime$ given density $\tilde{n}(z,t)$ at location z. As before, $\tilde{n}$ is a function of pop-

ulation structure – in our model, weighted local density – but here integrated over an

explicit competitive "neighborhood": $\tilde{n}(z,t) = \int_{z-h}^{z+h} \int_{L}^{U} xn(x,z,t) \, dx \, dz$ where h repre-

sents neighborhood size in the units of z.

Given that the shrub population at this site is approximately homogeneous perpen-

dicular to the direction of encroachment, expansion is modelled as a wave moving in one

dimension. A spatial integral projection model (SIPM) is used to estimate the speed at

which encroachment occurs; such a model incorporates the effects of variation in traits

like plant size that stage-structured models, such as those described in Neubert and

Caswell (2000), do not capture. According to Jongejans et al. (2011), a general SIPM

can be formulated as

$$\mathbf{n}(x_2, z_2, t+1) = \iint \tilde{K}(x_2, x_1, z_2, z_1) \mathbf{n}(x_1, z_1, t) \, dx_1 \, dz_1 \tag{9}$$

where x_1 and x_2 are locations of individuals of a particular size before and after one unit of

time, and z_1 and z_2 are the respective sizes. The vector $\mathbf{n}$ indicates the population density

of each size, and $\tilde{K}$ is a kernel that combines dispersal with demography. Though this

SIPM represents a continuous spectrum of shrub sizes and densities, it was implemented

by discretising the above integral with a 200 x 200 matrix, as this makes calculations

significantly more tractable.

Movement of the wave is determined by the components of the combined disper-

sal/demography kernel $\tilde{K}$, which is of the same form as that used in Jonjegans et al.

20

(2011). Here,

$$\tilde{K}(x_2, x_1, z_2, z_1) = K(x_2 - x_1)Q(z_2 - z_1) + \delta(x_2 - x_1)G(z_2 - z_1) \tag{10}$$

and K is the dispersal kernel, Q a reproduction function, G a growth function, and δ the Dirac delta function. G is derived from the model for annual growth ratio, and Q is derived from the reproductive structures model as well as other factors including number of seeds per reproductive structure, probability of recruitment from seed, and recruit size. Both G and Q give the probability of transition between sizes; in the case of G, this is the probability of growing from one specific size to another, and in the case of Q the probability that an individual of a specific size produces a recruit of a specific size. The product of K and Q represents the production and dispersal of motile propagules, while the product of G and δ represents the growth of sessile individuals.

Given growth function G and the reproduction function Q, the speed of the moving wave can be calculated as

$$c^* = \min_{s>0}\left[\frac{1}{s}\ln(\rho_s)\right] \tag{11}$$

where s is the wave shape parameter and ρ_s is the dominant eigenvalue of the kernel $\mathbf{H_S}$ (Jongejans et al., 2011). This estimate for the wavespeed is valid under the assumption that population growth decreases monotonically as conspecific density increases, with the highest rates of growth occurring at the lowest population densities (Lewis et al., 2006). The kernel $\mathbf{H_S}$ is defined as

$$\mathbf{H_S} = M(s)Q(z_2 - z_1) + G(z_2 - z_1) \tag{12}$$

where $M(s)$ is the moment-generating function of the dispersal kernel (Jongejans et al., 2011). For one-dimensional dispersal, this moment-generating function can be estimated

21

as

$$M(s) = \frac{1}{N} \sum_{i=1}^{n} I_0(sr_i) \tag{13}$$

where r is the dispersal distance for each observation, and I_0 is the modified Bessel function of the first kind and zeroth order (Skarpaas and Shea, 2007). In order to obtain M, numerous dispersal distances were simulated from the dispersal kernel $K(r)$ described in the previous section, with over 2000 replications for each shrub height increment of 1 cm. This was performed over the range from the lowest possible dispersal height to the maximum shrub height. Once $M(s)$ was obtained for dispersal at each shrub height, $\mathbf{H_S}$ and c^* were calculated for each value of s; this was done for values of s ranging from 0 to 2, as it is this range in which c^* occurs.

Estimates of the wavespeed were bootstrapped for a total of 1000 replicates. Each bootstrap replicate recreated size- and density-dependent demographic models using 80% resampling on the original demographic data, and recreated dispersal kernels also using 80% resampling on the wind speeds and seed terminal velocities. Between replicates, the structure of the demographic models was kept constant, though coefficient estimates were not; this approach, while effectively ignoring model uncertainty, has the benefit of increasing computational efficiency, which is especially useful given the time-consuming nature of numerically estimating the many dispersal kernels used in the model.

Results

Encroachment re-surveys

Re-surveys along two permanent transects revealed virtually no change the in the creosote expansion wave over 12 years (Fig. 2). There were local changes in percent cover: on average cover increased by XX% between surveys. However, there was no clear indication that the leading edge of the creosote shrubland has advanced (the modest right-ward shift on both transects is within the range of measurement error).
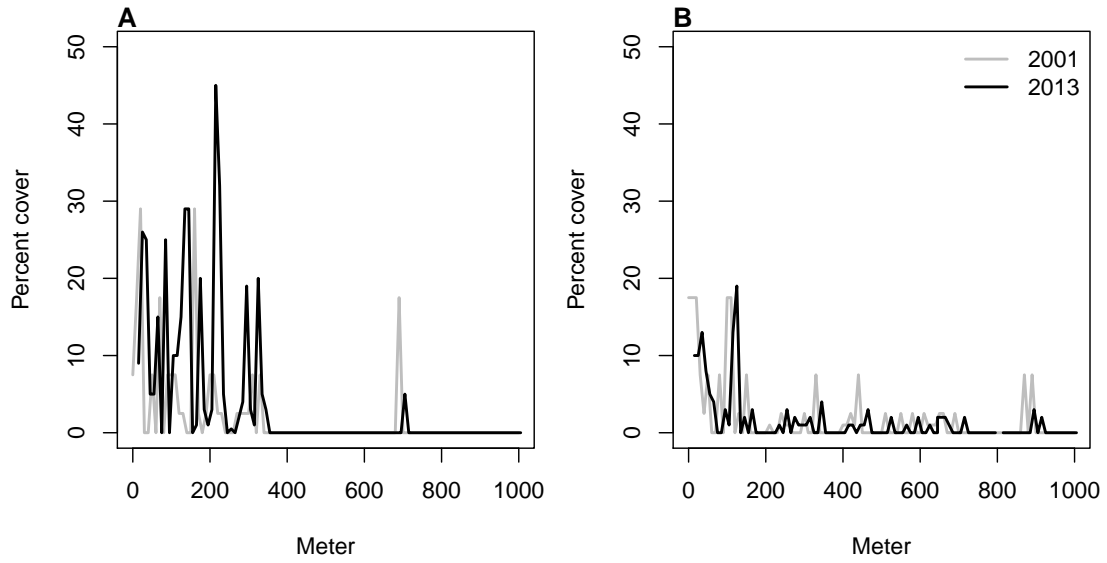
22

Figure 2: Re-surveys of shrub cover along two permanent trasects (A,B) surveyed in 2001 and 2013.

Size and density dependent demography

Demographic data from naturally occurring and transplanted individuals revealed strong size- and density-dependence in demographic vital rates. For most sizes and vital rates, local density had negative demographic effects. Statistical support for size- and density-dependence is provided in Table XX, which provides AIC rankings for candidate models based on the completed (not bootstrapped) data set.
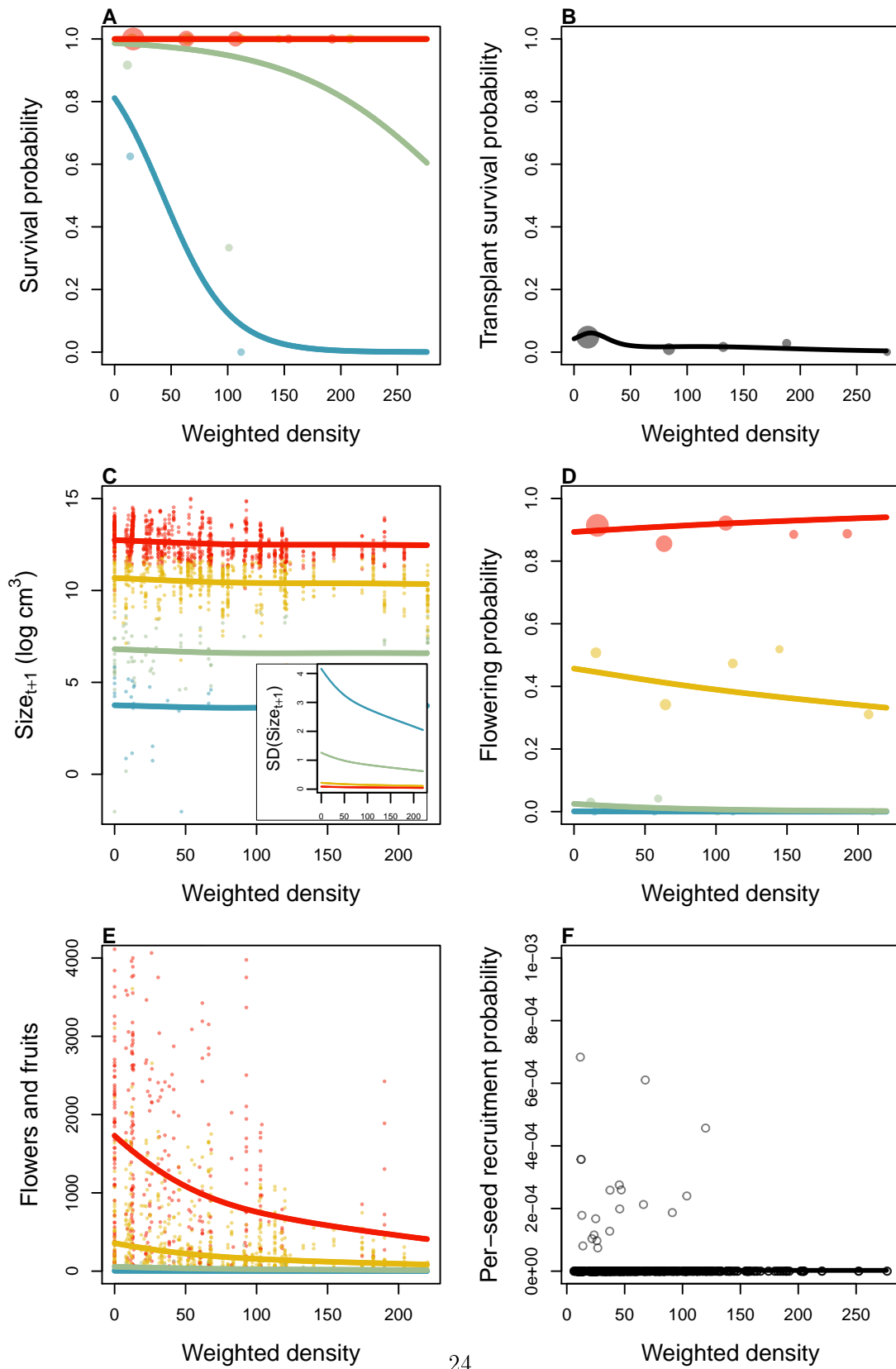
Figure 3: Size- and density-dependence in demographic vital rates.

24

Survival   Among naturally occurring plants, survival of large, established individuals was very high (Fig. 3A). We observed relatively few mortality events (XX out of XX) and nearly all of these were among new recruits that we detected during the study. The probability of survival at these small sizes declined with increasing density.

Survival of transplants was very low, lower even than survival of similarly-sized, naturally occurring recruits (Fig. 3B). However, the transplant results support the general pattern of negative density dependence in survival. Among the XX survivors, XX of them occurred in transect windows in the bottom 10th percentile of weighted shrub density.

SHORT PARAGRAPH SUMMARIZING SMALLER-SCALE ANALYSIS IN APPENDIX.

Growth   Current size was strongly predictive of future size, as expected, and there was weak negative density dependence in mean future size conditioned on current size (Fig. 3C). However, there was a stronger signal of density dependence in the standard deviation of future size (Fig. 3C, inset). Plants at low density exhibited greater variance in growth trajectories and this was especially true at the smallest sizes. Thus, large increases in the size of new recruits were most likely under low-density conditions.
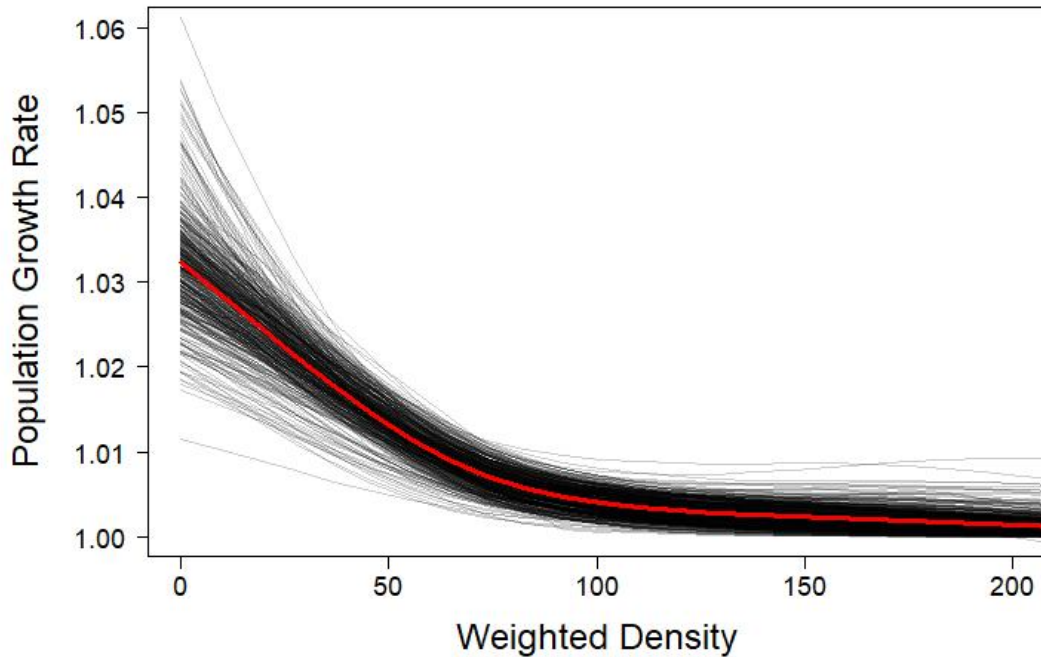
Flowering and fruit production

Recruitment

Figure 4: Density dependence in the geographic population growth rate (λ).

Population growth rate The speed of encroachment at the study site as estimated by the SIPM is rather slow; as can be seen in Figure 5, the low-density wavefront moves at approximately 0.5 cm/yr under normal conditions and at 1 cm/yr under the best seedling survival conditions observed in the dataset. These improved conditions were observed due to above-average rainfall that occurred after greenhouse-grown seedlings were transplanted to the site. Population growth in this low-density region of the moving wave is also low, with a geometric growth rate of $\lambda \approx 1.006$ and even lower rates of growth the higher-density regions behind; in the higher-survival scenario the maximum rate increases to $\lambda \approx 1.013$, with growth still decreasing as density increases. For both scenarios, the decrease in population growth rate with increasing density was monotonic across the range of observed standardised densities, as is shown in Figure 5. This suggests that an Allee effect is likely not present in this population, as the highest rate of popula-

26

tion growth is found at the lowest density vanguard of the encroaching population. Thus, the conditions necessary for equation 9 to be valid are satisfied, and these wavespeeds are applicable for a pulled-wave scenario in which no Allee effects are present.
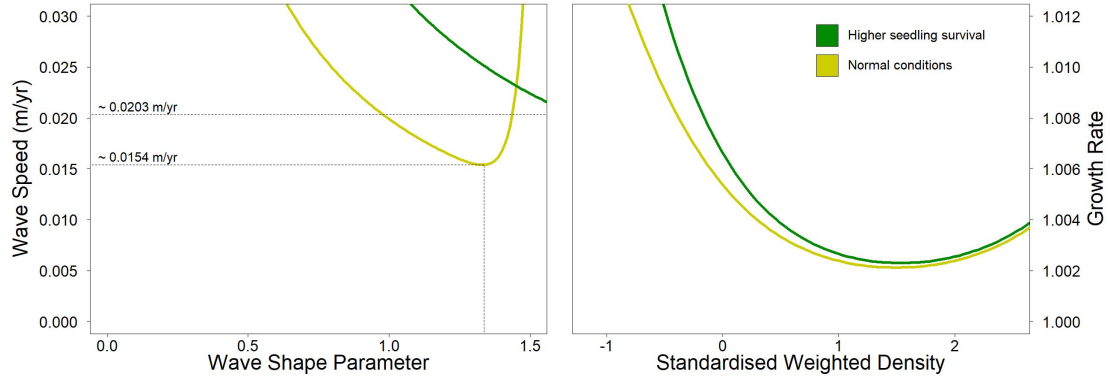

Figure 5: Estimated encroachment wave speeds (left) and geometric rates of population growth (right) for higher post-rainfall seedling survival and normal conditions.

As the speed of encroachment is quite limited, so is the extent of wind dispersal. Long distance dispersal events, while more common for taller shrubs than their shorter counterparts, are still uncommon overall. For the tallest shrub height of 1.98 m, only 0.32% of propagules exceed a dispersal distance of 5 m, and 0.02% exceed 10 m. At 1 m, or approximately half the tallest shrub height, long distance dispersal is even less likely, with 0.0046% of propagules exceeding a dispersal distance of 5 m and 0.0009% exceeding 10 m. Given that the median shrub height is only 0.64 m, the occurrence of long-distance wind dispersal in most of the shrub population is highly improbable, and the few instances in which it occurs will only be limited to the tallest shrubs. Thus, as Figure 6 demonstrates, shorter dispersal distances dominate; even for the tallest shrub, 81% of seeds fall within only a metre of the plant, and this percentage increases as shrub height decreases. Dispersal kernels have their highest probability density at dispersal distances between 2 and 8 cm from the shrub; here, as shrub height increases, the most probable dispersal distance slightly increases while maximum probability density

decreases. Regardless of the shrub height, most dispersal will occur very close to the plant, though increases in shrub height dramatically increase the likelihood of dispersal at longer distances. It is clear that the shape of the height-dependent dispersal kernel $K(r)$ varies greatly among the shrub population given the large range of shrub heights observed; shrubs at lower heights have more slender kernels with most of the seeds dispersing closer to the plant, while taller shrubs have kernels with much fatter tails and are more capable of longer-distance dispersal.
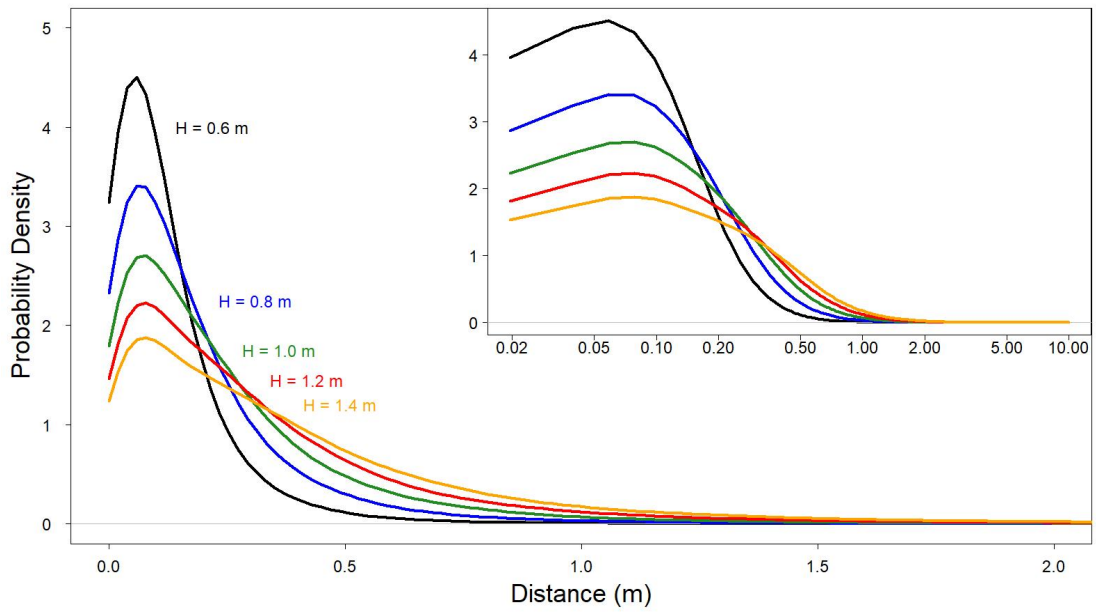

Figure 6: Dispersal kernels, with each colour representing a selected shrub height. The inset plot is the same as the large plot, though with a logarithmic x-axis to more easily show differences in dispersal probability at smaller distances.

Density and size dependence are evident in all 4 of the demographic rates, with coefficients for each model displayed in Table 2. For growth, reproduction, and survival, density dependence is mostly negative and monotonic; this is not the case for probability of flowering, where shrub size seems to be more important than the effects of density alone and suggests that larger shrubs have a higher probability of flowering than their smaller

counterparts. This, along with size and density dependence in growth and reproduction, is shown in Figure 7. Size dependence is positive for reproduction, as would be expected since larger plants typically produce more flowers and fruits. However, annual growth decreases as size increases; this could be in part due to the annual growth in this study being quantified as a proportion relative to the shrub's initial size. While larger shrubs may produce more plant material over a year in terms of absolute volume, smaller shrubs produce less but can still have higher annual growth in terms of the percentage of volume added relative to their initial volume. When compared to density, shrub size is a much stronger predictor of survival, with significant differences in mortality rates depending on shrub size. For small shrubs, mortality is exceptionally high, and increases in volume for these shrubs only slightly increase the likelihood of survival. However, after shrubs reach a logarithmic volume of approximately 7.3, they are almost guaranteed to survive, with survival rates near 100% persisting regardless of any further size increases. Interestingly, though most recruits were found at lower densities, the probability of recruitment from seed displays positive density dependence; the probability of recruitment was still very low, though, with a baseline rate of approximately 2 recruits per 10,000 seeds.
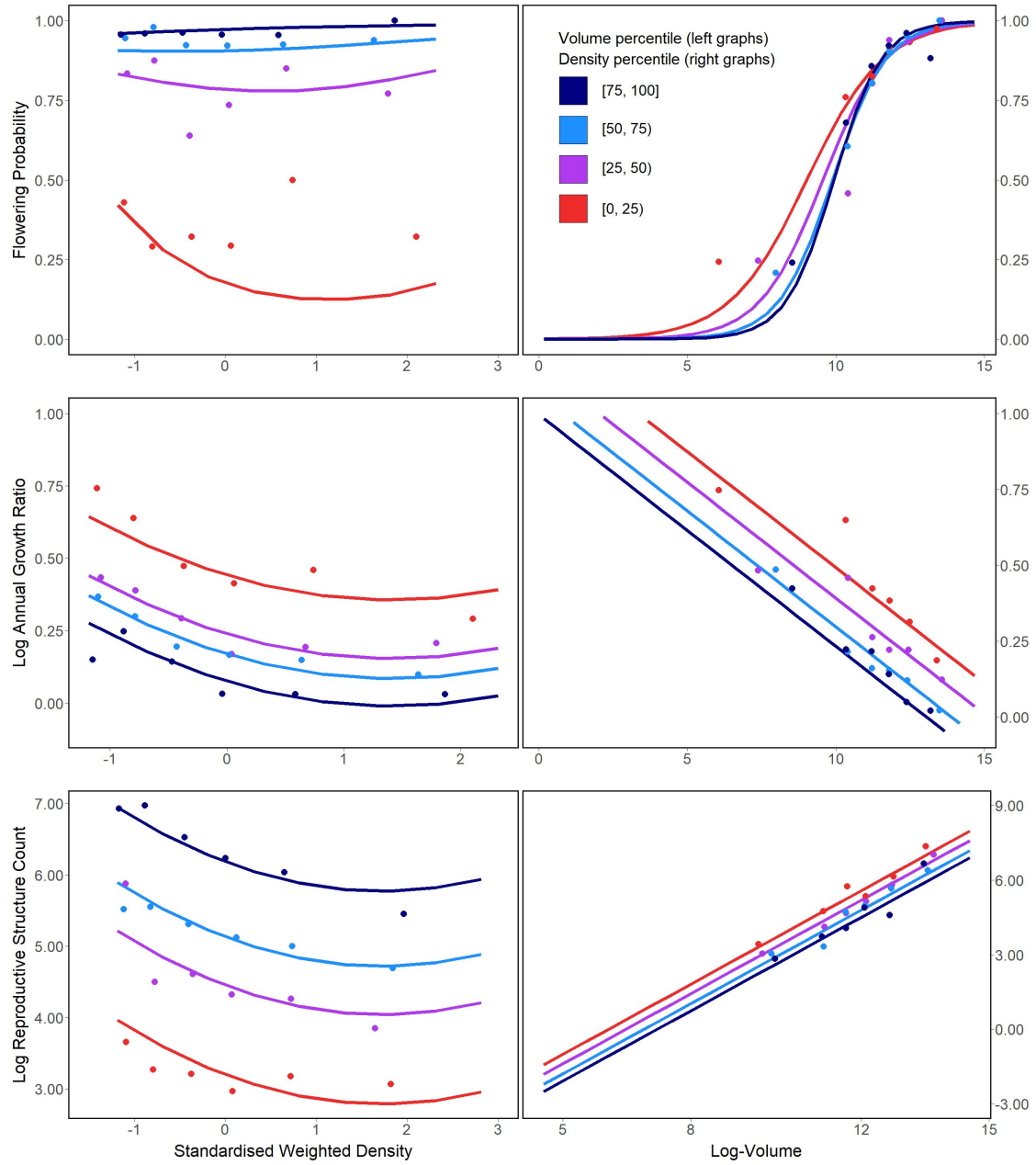
Figure 7: Flowering probability (top row), log annual growth ratio (centre row), and log reproductive structure count (bottom row) at all four sampling sites. In the left column of graphs, the three response variables are shown as a function of density for each of four volume quartiles, with each quartile containing six density bins; in the right column, the opposite occurs, with response variables shown as functions of four volume quartiles that each contain six density bins. Graphs quantifying the number of reproductive structures include data only on plants that flowered.

Discussion

The slow movement of the encroaching creosotebush wave at the Sevilleta LTER site can likely be contributed to a combination of three factors: short dispersal distances with extremely limited long-distance dispersal events, very low probability of recruitment from seed, and high seedling mortality. These three barriers, when combined, form a formidable challenge to the establishment of new shrubs at the low-density front of the wave. First, a seed must travel far enough to avoid competition with the parent shrub, which is unlikely given the dispersal kernels shown in Figure 2. Even if the seed manages to be dispersed this far, its chances of becoming a seedling are low. Caching and consumption by seed-eaters such as a variety of seed-harvesting ants (Whitford, 1978; Whitford et al., 1980; Lei, 1999) and the kangaroo rat Dipodomys merriami (Chew and Chew, 1970) decreases the amount of seeds available for germination. However, reduction in germination caused by destruction of seeds may be partly mitigated by the more favourable germination conditions that these seeds can experience when cached underground (Chew and Chew, 1970). Many of the remaining seeds will still fail to germinate, and in the unlikely event that germination does occur, seedlings will likely die given the high rates of mortality observed in smaller shrubs. Such high rates of creosotebush seedling mortality have been observed in other studies as well (Boyd and Brum, 1983; Bowers et al., 2004), probably due to a combination of herbivory, competition, and abiotic stresses.

However, as low as they are, the wavespeed estimates given in this paper are still conservative estimates for reasons mostly related to dispersal. First, it is important to note that the dispersal kernels used here, while they account for variation in factors such as wind speed and terminal velocity, may underestimate the distances that shrub propagules travel. Because the WALD model assumes that terminal velocity is reached immediately upon seed release, seeds in the estimate thus take a shorter time to fall

31

and have less time to be transported by wind, and the true frequency of long-distance dispersal events may thus be greater than what is estimated here. Second, dispersal at the study site could occur through additional mechanisms other than wind. For example, secondary dispersal through runoff from significant rainfall events can transport seeds (Thompson et al., 2014), and given that long-distance dispersal by bird and subsequent species divergence is thought to be responsible for creosotebush being in North America in the first place (Wells and Hunziker, 1976), short-distance dispersal by other animals at the study site likely occurs. As mentioned above, seeds are transported by seed-harvesting ants and granivorous mammals, where they are often stored in caches that can be appreciable distances from the parent shrubs. Whether transportation occurs via ant or rodent, creosotebush seeds can be moved significantly further than wind alone can, though many of these seeds are eventually consumed.

Despite the more conservative estimates our model yields, the estimated rate of dispersal in creosotebush populations at the Sevilleta National Wildlife Refuge is consistent with observations from the past 50-60 years, as creosotebush expansion during this time has been minimal (Moreno-de las Heras et al., 2016). However, it cannot explain the long-term increases in creosotebush cover at the study site, as total encroachment over the past 150 years is much greater than what would be expected given the encroachment rates derived by our models. Such a discrepancy is likely due to much of the expansion occurring in an episodic fashion, with short times during which rapid encroachment occurs due to favourable environmental conditions. This could be due in part to seedling recruitment, which is a factor that strongly limits creosotebush expansion, being rare and episodic. For example, Allen et al. (2008) estimate that a major recruitment event occurred at this site in the 1950s, which is supported by photographic evidence from Milne et al. (2003) of a drought-driven expansion during this time. Moreno-de las Heras et al. (2016) estimate that after this expansion, several smaller creosotebush recruitment events occurred in decadal episodes. However, such events can be highly localised and

may not necessarily occur at the low-density front of encroachment, which could explain how these recruitment events can still coexist with lack of encroachment in the recent past.

Overall, our observations and model highlight three aspects of creosotebush encroachment that should be the focus of future studies seeking to obtain better estimates of encroachment rates. First, negative density dependence in survival, growth, and reproduction is demonstrated, along with size dependence. The clear dependence on size and conspecific density suggests that they both should be considered when estimating creosotebush expansion and quantifying the demographic variation that contributes to it. Second, wind dispersal in these shrubs is quite limited; though the dispersal kernels seen here are typical in the sense that they are characterised by high near-plant dispersal and exceptionally low long-distance dispersal, the scale across which such dispersal occurs is small, with most seeds landing within only 1 m of the shrub. Wind dispersal alone may be an underestimate of the true amount of dispersal occurring, and future work should seek to incorporate the effects of dispersal by runoff and animals so that a more representative model of total dispersal can be obtained. Finally, encroachment is slow or even stagnates, but only most of the time. Though our encroachment speed estimates are representative of creosotebush populations for most years, the significant expansion seen over larger time scales suggests that there is episodic expansion in other years; while our model is consistent with the recent stagnation in creosotebush encroachment at the Sevilleta LTER site, a model that also includes interannual variability in factors such as survival and recruitment would be able to better account for instances of episodic population expansion that are characteristic of this location.

Acknowledgements

Author contributions

Data accessibility

References

Allen, A., W. Pockman, C. Restrepo, and B. Milne. 2008. Allometry, growth and population regulation of the desert shrub Larrea tridentata. Functional Ecology pages 197–204.

Bowers, J. E., R. M. Turner, and T. L. Burgess. 2004. Temporal and spatial patterns in emergence and early survival of perennial plants in the Sonoran Desert. Plant Ecology **172**:107–119.

Boyd, R. S., and G. D. Brum. 1983. Postdispersal reproductive biology of a Mojave Desert population of Larrea tridentata (Zygophyllaceae). American Midland Naturalist pages 25–36.

Brandt, J. S., M. A. Haynes, T. Kuemmerle, D. M. Waller, and V. C. Radeloff. 2013. Regime shift on the roof of the world: Alpine meadows converting to shrublands in the southern Himalayas. Biological Conservation **158**:116–127.

Buffington, L. C., and C. H. Herbel. 1965. Vegetational changes on a semidesert grassland range from 1858 to 1963. Ecological monographs **35**:139–164.

Bullock, J. M., S. M. White, C. Prudhomme, C. Tansey, R. Perea, and D. A. Hooftman. 2012. Modelling spread of British wind-dispersed plants under future wind speeds in a changing climate. Journal of Ecology **100**:104–115.

Cabral, A., J. De Miguel, A. Rescia, M. Schmitz, and F. Pineda. 2003. Shrub encroach-
ment in Argentinean savannas. Journal of Vegetation Science **14**:145–152.

Chew, R. M., and A. E. Chew. 1970. Energy relationships of the mammals of a desert
shrub (Larrea tridentata) community. Ecological Monographs pages 2–21.

Davis, C., 2015. sgt: Skewed Generalized T Distribution Tree. URL `https://CRAN.`
`R-project.org/package=sgt`.

D'Odorico, P., J. D. Fuentes, W. T. Pockman, S. L. Collins, Y. He, J. S. Medeiros,
S. DeWekker, and M. E. Litvak. 2010. Positive feedback between microclimate and
shrub encroachment in the northern Chihuahuan desert. Ecosphere **1**:1–11.

D'Odorico, P., G. S. Okin, and B. T. Bestelmeyer. 2012. A synthetic review of feedbacks
and drivers of shrub encroachment in arid grasslands. Ecohydrology **5**:520–530.

Gandhi, S. R., E. A. Yurtsev, K. S. Korolev, and J. Gore. 2016. Range expansions
transition from pulled to pushed waves as growth becomes more cooperative in an
experimental microbial population. Proceedings of the National Academy of Sciences
113:6922–6927.

Gardner, J. L. 1951. Vegetation of the creosotebush area of the Rio Grande Valley in
New Mexico. Ecological Monographs **21**:379–403.

Gibbens, R., R. McNeely, K. Havstad, R. Beck, and B. Nolen. 2005. Vegetation changes
in the Jornada Basin from 1858 to 1998. Journal of Arid Environments **61**:651–668.

Goslee, S., K. Havstad, D. Peters, A. Rango, and W. Schlesinger. 2003. High-resolution
images reveal rate and pattern of shrub encroachment over six decades in New Mexico,
USA. Journal of Arid Environments **54**:755–767.

Grover, H. D., and H. B. Musick. 1990. Shrubland encroachment in southern New Mexico,

USA: an analysis of desertification processes in the American Southwest. Climatic change **17**:305–330.

Hsieh, C.-I., and G. G. Katul. 1997. Dissipation methods, Taylor's hypothesis, and stability correction functions in the atmospheric surface layer. Journal of Geophysical Research: Atmospheres **102**:16391–16405.

Huang, H., L. D. Anderegg, T. E. Dawson, S. Mote, and P. D'Odorico. 2020. Critical transition to woody plant dominance through microclimate feedbacks in North American coastal ecosystems. Ecology **101**:e03107.

Jongejans, E., K. Shea, O. Skarpaas, D. Kelly, and S. P. Ellner. 2011. Importance of individual and environmental variation for invasive species spread: a spatial integral projection model. Ecology **92**:86–97.

Katul, G., A. Porporato, R. Nathan, M. Siqueira, M. Soons, D. Poggi, H. Horn, and S. A. Levin. 2005. Mechanistic analytical models for long-distance seed dispersal by wind. The American Naturalist **166**:368–381.

Keitt, T. H., M. A. Lewis, and R. D. Holt. 2001. Allee effects, invasion pinning, and species' borders. The American Naturalist **157**:203–216.

Kelleway, J. J., K. Cavanaugh, K. Rogers, I. C. Feller, E. Ens, C. Doughty, and N. Saintilan. 2017. Review of the ecosystem service implications of mangrove encroachment into salt marshes. Global Change Biology **23**:3967–3983.

Knapp, A. K., J. M. Briggs, S. L. Collins, S. R. Archer, M. S. BRET-HARTE, B. E. Ewers, D. P. Peters, D. R. Young, G. R. Shaver, E. Pendall, et al. 2008. Shrub encroachment in North American grasslands: shifts in growth form dominance rapidly alters control of ecosystem carbon inputs. Global Change Biology **14**:615–623.

36

Kot, M., M. A. Lewis, and P. van den Driessche. 1996. Dispersal data and the spread of invading organisms. Ecology **77**:2027–2042.

Lei, S. A. 1999. Ecological impacts of Pogonomyrmex on woody vegetation of a Larrea-Ambrosia shrubland. The Great Basin Naturalist pages 281–284.

Lewis, M., and P. Kareiva. 1993. Allee dynamics and the spread of invading organisms. Theoretical Population Biology **43**:141–158.

Lewis, M. A., M. G. Neubert, H. Caswell, J. S. Clark, and K. Shea, 2006. A guide to calculating discrete-time invasion rates from data. Pages 169–192 *in* Conceptual ecology and invasion biology: reciprocal approaches to nature. Springer.

Mabry, T. J., J. H. Hunziker, D. Difeo Jr, et al. 1978. Creosote bush: biology and chemistry of Larrea in New World deserts. Dowden, Hutchinson & Ross, Inc.

Maddox, J. C., and S. Carlquist. 1985. Wind dispersal in Californian desert plants: experimental studies and conceptual considerations. Aliso: A Journal of Systematic and Evolutionary Botany **11**:77–96.

Milne, B. T., D. I. Moore, J. L. Betancourt, J. A. Parks, T. W. Swetnam, R. R. Parmenter, and W. T. Pockman. 2003. Multidecadal drought cycles in south-central New Mexico: Patterns and consequences. Oxford University Press: New York, NY.

Moreno-de Las Heras, M., R. Díaz-Sierra, L. Turnbull, and J. Wainwright. 2015. Assessing vegetation structure and ANPP dynamics in a grassland–shrubland Chihuahuan ecotone using NDVI–rainfall relationships. Biogeosciences **12**:2907–2925.

Moreno-de las Heras, M., L. Turnbull, and J. Wainwright. 2016. Seed-bank structure and plant-recruitment conditions regulate the dynamics of a grassland-shrubland Chihuahuan ecotone. Ecology **97**:2303–2318.

Mugasi, S., E. Sabiiti, and B. Tayebwa. 2000. The economic implications of bush encroachment on livestock farming in rangelands of Uganda. African Journal of Range and Forage Science **17**:64–69.

Nathan, R., G. G. Katul, G. Bohrer, A. Kuparinen, M. B. Soons, S. E. Thompson, A. Trakhtenbrot, and H. S. Horn. 2011. Mechanistic models of seed dispersal by wind. Theoretical Ecology **4**:113–132.

Neubert, M. G., and H. Caswell. 2000. Demography and dispersal: calculation and sensitivity analysis of invasion speed for structured populations. Ecology **81**:1613–1628.

Oba, G., E. Post, P. Syvertsen, and N. Stenseth. 2000. Bush cover and range condition assessments in relation to landscape and grazing in southern Ethiopia. Landscape ecology **15**:535–546.

Pan, S., and G. Lin. 2012. Invasion traveling wave solutions of a competitive system with dispersal. Boundary Value Problems **2012**:120.

Parizek, B., C. M. Rostagno, and R. Sottini. 2002. Soil erosion as affected by shrub encroachment in northeastern Patagonia. Rangeland Ecology & Management/Journal of Range Management Archives **55**:43–48.

Peters, D. P., and J. Yao. 2012. Long-term experimental loss of foundation species: consequences for dynamics at ecotones across heterogeneous landscapes. Ecosphere **3**:1–23.

Ratajczak, Z., J. B. Nippert, and S. L. Collins. 2012. Woody encroachment decreases diversity across North American grasslands and savannas. Ecology **93**:697–703.

Raupach, M. 1994. Simplified expressions for vegetation roughness length and zero-

767   plane displacement as functions of canopy height and area index. Boundary-Layer

768   Meteorology **71**:211–216.

769   Ravi, S., P. D'Odorico, S. L. Collins, and T. E. Huxman. 2009. Can biological invasions

770   induce desertification? The New Phytologist **181**:512–515.

771   Reed, M., L. Stringer, A. Dougill, J. Perkins, J. Atlhopheng, K. Mulale, and N. Favretto.

772   2015. Reorienting land degradation towards sustainable land management: Linking

773   sustainable livelihoods with ecosystem services in rangeland systems. Journal of envi-

774   ronmental management **151**:472–485.

775   Reynolds, J. F., R. A. Virginia, P. R. Kemp, A. G. De Soyza, and D. C. Tremmel. 1999.

776   Impact of drought on desert shrubs: effects of seasonality and degree of resource island

777   development. Ecological Monographs **69**:69–106.

778   Roques, K., T. O'connor, and A. R. Watkinson. 2001. Dynamics of shrub encroach-

779   ment in an African savanna: relative influences of fire, herbivory, rainfall and density

780   dependence. Journal of Applied Ecology **38**:268–280.

781   Schlesinger, W. H., and A. M. Pilmanis. 1998. Plant-soil interactions in deserts. Biogeo-

782   chemistry **42**:169–187.

783   Schlesinger, W. H., J. A. Raikes, A. E. Hartley, and A. F. Cross. 1996. On the spatial

784   pattern of soil nutrients in desert ecosystems: ecological archives E077-002. Ecology

785   **77**:364–374.

786   Schlesinger, W. H., J. F. Reynolds, G. L. Cunningham, L. F. Huenneke, W. M. Jarrell,

787   R. A. Virginia, and W. G. Whitford. 1990. Biological feedbacks in global desertification.

788   Science **247**:1043–1048.

789   Sirami, C., and A. Monadjem. 2012. Changes in bird communities in Swaziland savannas

between 1998 and 2008 owing to shrub encroachment. Diversity and Distributions **18**:390–400.

Skarpaas, O., and K. Shea. 2007. Dispersal patterns, dispersal mechanisms, and invasion wave speeds for invasive thistles. The American Naturalist **170**:421–430.

Sullivan, L. L., B. Li, T. E. Miller, M. G. Neubert, and A. K. Shaw. 2017. Density dependence in demography and dispersal generates fluctuating invasion speeds. Proceedings of the National Academy of Sciences **114**:5053–5058.

Taylor, C. M., and A. Hastings. 2005. Allee effects in biological invasions. Ecology Letters **8**:895–908.

Thompson, S. E., S. Assouline, L. Chen, A. Trahktenbrot, T. Svoray, and G. G. Katul. 2014. Secondary dispersal driven by overland flow in drylands: Review and mechanistic model development. Movement ecology **2**:7.

Trollope, W., F. Hobson, J. Danckwerts, and J. Van Niekerk. 1989. Encroachment and control of undesirable plants. Veld management in the Eastern Cape pages 73–89.

Turnbull, L., J. Wainwright, and R. E. Brazier. 2010. Changes in hydrology and erosion over a transition from grassland to shrubland. Hydrological Processes: An International Journal **24**:393–414.

Van Auken, O. 2009. Causes and consequences of woody plant encroachment into western North American grasslands. Journal of environmental management **90**:2931–2942.

Van Auken, O. W. 2000. Shrub invasions of North American semiarid grasslands. Annual review of ecology and systematics **31**:197–215.

Vasek, F. C. 1980. Creosote bush: Long-lived clones in the Mojave Desert. American Journal of Botany **67**:246–255.

Veit, R. R., and M. A. Lewis. 1996. Dispersal, population growth, and the Allee effect: dynamics of the house finch invasion of eastern North America. The American Naturalist **148**:255–274.

Wang, M.-H., M. Kot, and M. G. Neubert. 2002. Integrodifference equations, Allee effects, and invasions. Journal of mathematical biology **44**:150–168.

Wells, P. V., and J. H. Hunziker. 1976. Origin of the creosote bush (Larrea) deserts of southwestern North America. Annals of the Missouri Botanical Garden pages 843–861.

Whitford, W., E. Depree, and P. Johnson. 1980. Foraging ecology of two chihuahuan desert ant species: Novomessor cockerelli andNovomessor albisetosus. Insectes Sociaux **27**:148–156.

Whitford, W. G. 1978. Structure and seasonal activity of Chihuahua desert ant communities. Insectes Sociaux **25**:79–88.

Wiernga, J. 1993. Representative roughness parameters for homogeneous terrain. Boundary-Layer Meteorology **63**:323–363.

Williams, J. L., T. E. Miller, and S. P. Ellner. 2012. Avoiding unintentional eviction from integral projection models. Ecology **93**:2008–2014.

Wood, S. 2017. Generalized Additive Models: An Introduction with R. 2 edition. Chapman and Hall/CRC.

831 Appendix A